THE JOURNAL OF PHYSICAL CHEMISTRY B

Article

Cite This: J. Phys. Chem. B 2018, 122, 6616−6626

pubs.acs.org/JPCB

Understanding the Role of Hydrophobic Terminal in the Hydrogen Bond Network of the Aqueous Mixture of 2,2,2-Trifluoroethanol: IR, Molecular Dynamics, Quantum Chemical as Well as Atoms in Molecules Studies

Saptarsi Mondal, Biswajit Biswas, Tonima Nandy, and Prashant Chandra Singh*

Department of Spectroscopy, Indian Association for the Cultivation of Science, Kolkata 700032, India

Supporting Information

ABSTRACT: The aqueous mixture of 2,2,2-trifluoroethanol (TFE) is one of the important alcoholic solvents which has been extensively used for understanding the stability of proteins as well as several chemical reactions. In this paper, the deconvolution of the IR lines in the OH-stretching region has been applied to understand the local structure of water−water, alcohol−water, and alcohol−alcohol interactions in the water mixture of TFE and ethanol (ETH). Further, molecular dynamics simulations, quantum chemical calculations, and atoms in molecules analysis have been performed to encode the local structure information obtained from the experimental data. Addition of a small amount of alcohol in a pure aqueous medium enhances the aggregation of water molecules for the case of ETH, whereas the hydrogen bond between TFE and water is the dominant contributor for TFE. The $-CF_3$ substitution changes the orientation and hydrogen-bonding site of water molecules from the hydrophilic OH terminal to the hydrophobic $-CF_3$ terminal of TFE, which decreases the clustering of water molecules as well as enhances the hydrogen bonding between TFE and water. In the TFE-rich region of the water mixture of TFE, the fluorine of the TFE molecules interacts with each other through a weak fluorous interaction which reduces the hydrogen bonding between the $-CF_3$ of TFE and water molecules. These findings about the hydrogen bond network of the water mixture of TFE induced by the hydrophobic $-CF_3$ group provide a stepwise explanation of the unique hydrophobic properties of the trifluoromethyl group containing pharmaceutical molecules.

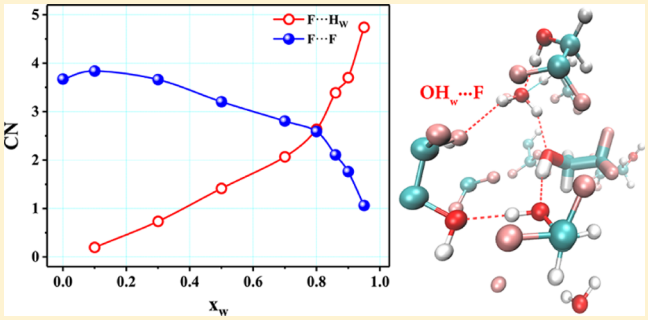

1. INTRODUCTION

2,2,2-Trifluoroethanol (TFE) is one of the most important fluorinated alcohol which has diverse applications such as reaction medium,[1−3] catalysis,[4−6] medicinal chemistry,[7,8] polymer synthesis,[9,10] and separation technique.[11−16] The presence of the $-CF_3$ group in TFE provides them with useful physicochemical properties as compared to the nonfluorinated analogs. The bond length as well as the dipole moment of the C−F bond is higher than that of C−H, and the direction of the dipole is opposite to that of the C−H group. In addition, the high electronegativity and smaller size of fluorine make the C−F group less polarizable than the C−H group. Hence, by virtue of the distinct properties of the C−F group, fluorinated molecules are extremely hydrophobic, inert, as well as prefer to self-aggregate through the weak fluorous (F···F) interactions.[17−21]

Indeed, it has been found that the aqueous mixture of TFE stabilizes the secondary structure of protein more as compared to the nonfluorinated alcohols and water.[15] On the basis of several simulations and experimental studies, it has been proposed that TFE displaces more water near to the proteins as compared to the nonfluorinated alcohols which enhances the probability of hydrogen bond formation between protein molecules, resulting in the stabilization of the secondary structure of proteins.[15,22] In another study, it has been shown that molecules containing the C−F group get more stabilized in TFE because of the weak fluorous interaction between the C−F group of the probe and the TFE molecule.[23,24] It has also been observed that the selectivity and yield of several reactions are increased when the reactions are performed in the aqueous mixture of TFE than in nonfluorinated alcohols.[4,25]

Because of these unique and important properties of the aqueous mixture of TFE, numerous theoretical and experimental studies have been performed to realize its different physical and biological properties.[12,26−31] The nuclear magnetic resonance (NMR), X-ray, and neutron scattering studies have shown that the aggregation of TFE is more than that of the nonfluorinated alcohols in their water mixtures.[32−35] Partial molar volume, density, and other thermodynamic properties of the aqueous mixture of TFE show deviation from the ideal behavior. Chitra and Smith performed the molecular dynamics

Received: May 8, 2018
Published: May 30, 2018

DOI: 10.1021/acs.jpcb.8b04365
J. Phys. Chem. B 2018, 122, 6616−6626

(MD) simulations on the aqueous mixture of TFE and reproduced most of the experimental thermodynamic data and concluded that the aggregation of TFE causes the deviation from the ideal behavior.[28,36] Jalili and Akhavan studied the hydrogen bond structure of the TFE−water mixture using the MD simulations and concluded that the hydrogen bond between TFE and water is broken when TFE is diluted with water.[17] The aggregation of TFE in their aqueous mixture is well-established; however, the extensive information about the role of the hydrophobic fluorine terminal ($-CF_3$) on the interaction with water and its effect on the hydrogen bond network is still not very clear.

In this paper, we have studied the aqueous mixture of TFE and ethanol (ETH) using infrared (IR) spectroscopy in the OH-stretching region and the MD simulation method to understand the role of different binding sites of alcohols in the evolution of their hydrogen bond network. The OH-stretching frequency is extremely sensitive to the local hydrogen bond environment and has been used earlier to realize the hydrogen bond network of many complex liquids and their mixtures.[37−40] The IR and MD studies combinedly reveal that the hydrophobic $-CF_3$ group of TFE causes a switch in the hydrogen-bonding site of the water molecules from the OH to the $-CF_3$ end of TFE which increases the $O-H_{TFE}\cdots O_w$ hydrogen bond between TFE and the water molecules and decreases the clustering of the water molecules via the $O-H_w\cdots O_w$ hydrogen bond, in contrast to the ETH−water mixture where the clustering of the water molecules dominate. The fluorous interaction between the fluorine of the TFE molecules dominates in the TFE-rich region which reduces the hydrogen bonding between water and the fluorine of TFE.

2. METHODS

The IR spectra of the aqueous mixtures of ETH and TFE in their OH-stretching regions were measured by the Fourier transform infrared spectrometer (Nicolet iS10, Thermo Fisher) working in the attenuated total reflection (ATR) mode. N_2 gas was flown to avoid the effect of the atmospheric vapors on the measurements. The resolution of the instrument was 2 cm^{-1}. The measured IR spectra have been corrected for ATR. All the experiments were performed at room temperature (26 ± 4 °C). ETH (99.9%) and TFE (99.9%) were purchased from Spectrochem (Mumbai, India) and dried using a molecular sieve prior to all measurements. To assure that pure alcohols are not contaminated by moisture, we measured the IR spectra of pure alcohols in the bending region of water. The aqueous mixtures of ETH and TFE were prepared by using Milli-Q water (H_2O, Millipore, 18.3 MΩ cm resistivity).

MD simulations of the water mixtures of ETH and TFE were carried out using two different all-atom simulation methods using the GROMACS MD simulation package.[41] All-atom optimized potentials for liquid simulations (OPLS) and Amber99sb-ildn force field parameters for ETH were used as available in GROMACS topology. The water model has been described by TIP3P for the OPLS force field, whereas TIP5PE was used for the Amber99sb-ildn force field. The OPLS force field parameters for TFE were adopted from Duffy et al.[42], whereas those of the Amber99sb-ildn force field were adopted from Gerig et al.[43] First, each trajectory was equilibrated in an NVT ensemble at 800 K for 500 ps to remove the biased dependencies on the initial configuration followed by an equilibration in an NPT ensemble at 300 K temperature and 1 bar pressure for 1 ns. Further, the production run of the equilibrated configuration was performed for another 5 ns in the NPT ensemble at 300 K and 1 bar pressure. The temperature and pressure were kept constant using the Berendsen thermostat[44] with a time constant (τ) of 0.1 ps and the Parrinello−Rahman barostat[45] with a τ of 1.0 ps, respectively. The particle mesh Ewald method was used for the incorporation of the electrostatic interactions.[46] The periodic boundary condition was used for each MD run with two femtoseconds time step. The nonbonded force calculation with a grid, updated after five steps, was used for the neighbor list generation. The neighbor list generation and van der Waal's interaction were calculated with a cutoff radius of 1.2 nm.

The performance of the force fields was checked by the calculation of the volumetric properties (molar volume of neat liquids, partial molar volume, and excess volume of mixing) and enthalpy of mixing and comparing them with the existing simulation as well as the experimental results (Tables S1−S15). The simulated values of density, molar volume, and molar enthalpy of pure liquids using these two force fields are in good agreement with the experimental values. It can be seen that the values of density, partial molar volume, and the excess molar volumes of the aqueous mixtures of ETH and TFE estimated from the Amber99sb-ildn force field are closer to their respective experimental values than the OPLS case. The dielectric constant of the alcohol−water mixture estimated from the Amber99sb-ildn force field is in good agreement with the experimental value in the water-rich region of the mixture, whereas the OPLS force field estimates the correct dielectric constant value in the alcohol-rich region of the mixture. The sign of the molar enthalpy of mixing of the ETH−water mixture has been estimated correctly by both the force fields; however, the minima have been correctly reproduced by the OPLS force field. The sign of the molar enthalpy of mixing of the TFE−water mixture has been correctly estimated by the OPLS force field, whereas the Amber99sb-ildn force field overestimates the values of molar enthalpy of mixing and provides the opposite sign. It is evident from the calculations that the volumetric properties are better estimated by Amber99sb-ildn, whereas the OPLS force field estimates more accurately the molar enthalpy of mixing. Nevertheless, the radial distribution functions of the different interacting groups providing the information about the hydrogen bond network of the water mixtures of ETH and TFE obtained from these two force fields show a similar trend, except that the aggregation of water in the alcohol-rich region is higher for OPLS as compared to the Amber99sb-ildn force field.

The B3LYP method and the 6-311+G(d,p) basis set were used for the optimization of the different types of clusters of ETH−water and TFE−water in their respective bulk media. The polarizable continuum model has been used to realize the solvent effect in the calculation. The frequency calculations of each optimized structure were performed to ensure that the optimized structures are minimum-energy structures. Standard convergence criteria and frozen core approximation were used for the optimization. The G09 suites of the program were used for all the calculations.[48] To understand the nature of interaction between the two groups, atoms in molecules (AIM) analysis was performed.[47]

3. RESULTS AND DISCUSSION

3.1. IR Study and the Deconvolution of the Bands.

The IR spectral feature of the water mixtures of alcohol in their OH-stretching region covering the range of 3000−3800 cm^{-1} is

DOI: 10.1021/acs.jpcb.8b04365
J. Phys. Chem. B 2018, 122, 6616−6626

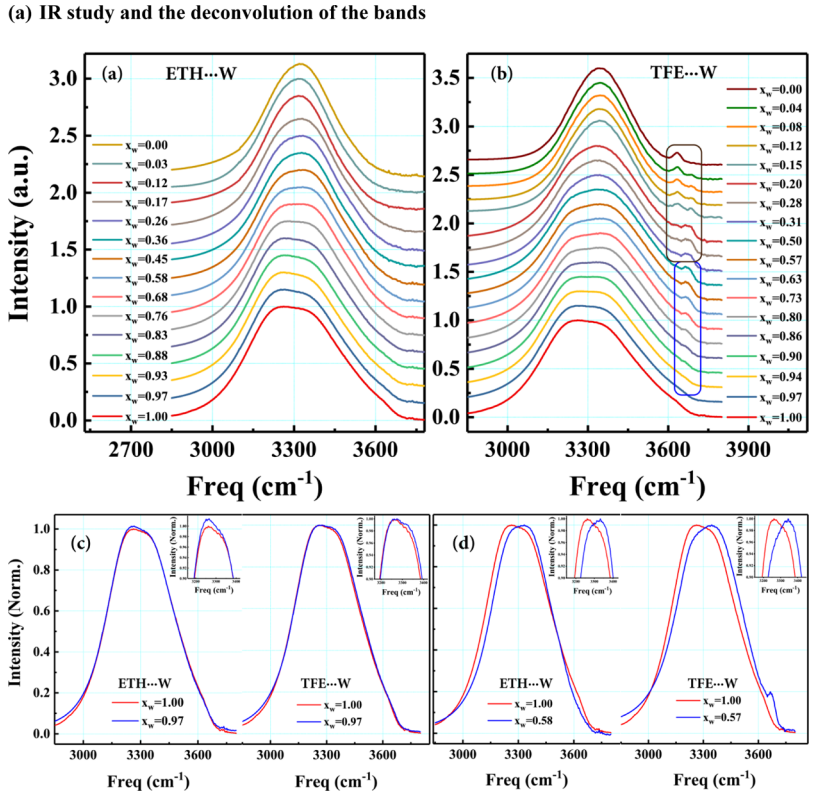

Figure 1. IR spectra in the OH-stretching region for different compositions of the water mixture of ETH (a) and TFE (b). The offset has been provided for clarity. (c,d) To find the difference in the band shape, the normalized IR spectra of the ETH−water and the TFE−water mixtures for two different compositions in the OH-stretching region with respect to pure water have been shown. The change in the band shape has also been shown in the insets of (c,d) for clarity of visualization.

depicted in Figure 1. The IR spectrum of bulk water shows two peak features centered at 3260 and 3370 cm^{-1} (Figure 1a,b, red line). The origin of the double-peak features of water has been controversial. Some groups believe that the spectral feature at ~3200 cm^{-1} belongs to the water molecules in the symmetrical tetrahedral hydrogen bond network and the peak at 3370 cm^{-1} is assigned to the asymmetric tetrahedral hydrogen-bonded network.[36] In contrast, the other groups believe that the double-peak feature of water originates from the Fermi resonance between the stretching and bending modes of the water molecules.[38,40] Bulk ETH shows a broad single IR peak at 3330 cm^{-1} (Figure 1a, dark yellow), which depicts the absence of Fermi resonance in bulk ETH. Bulk TFE shows a broad IR peak centered at ~3341 cm^{-1} along with a comparatively narrow-band feature at ~3634 cm^{-1} (Figure 1b, brown line). In our previous study, the broad IR feature below 3600 cm^{-1} has been assigned to the different sizes of the $O-H_{TFE}\cdots O_{TFE}$ hydrogen-bonded clusters of TFE and the narrow feature at the high-frequency region of the OH spectrum (~3634 cm^{-1}) has been attributed to the $O-H_{TFE}\cdots F_{TFE}$ interaction mainly originating from the dimer and trimer of the TFE clusters.[49] The IR feature of the bulk TFE at ~3634 cm^{-1} is relatively broad as well as slightly red-shifted compared to the IR spectrum of TFE in the isolated gas phase (~3651 cm^{-1}) which also justifies the assignment of this band to the weakly hydrogen-bonded $O-H_{TFE}\cdots F_{TFE}$ species (Figure S1).[50] The IR spectrum of TFE is more broad and blue-shifted than that of ETH, suggesting that the average hydrogen bond strength of the bulk TFE is less than that of the bulk ETH. In fact, a significant number of $O-H_{TFE}\cdots F_{TFE}$ interactions appear at the cost of $O-H_{TFE}\cdots O_{TFE}$ in the bulk TFE, resulting in a decrease in its average hydrogen bond strength.

The hydrogen bonds among the different species of alcohol−water mixtures compete throughout different compositions which determine the shape of the IR spectra in the OH-stretching regions. To discuss the role of all the contributors in the IR spectra, the aqueous mixtures of alcohols have been divided into three regions: (a) water-rich region ($X_w > 0.80$), (b) intermediate region ($0.80 \geq X_w \geq 0.20$), and (c) alcohol-rich region ($X_w < 0.20$). Two important parameters of the spectra, namely, the intensity change (depicting the change in the relative number of clusters) and the shift in the band position (depicting the average strength of the hydrogen bonds calculated over all the OH stretches) have been discussed to understand the hydrogen bond network of the water mixtures of ETH and TFE. In the water-rich region of the ETH−water mixture, the intensity ratio of the peaks at 3200 and 3370 cm^{-1} is increased more than that of pure bulk water, indicating that the overall spectra get red-shifted (clearly shown in the first plot of Figure 1c). In the water-rich region, either water can aggregate through the formation of strong $O-H_w\cdots O_w$ hydrogen bonds or intermolecular hydrogen bonds between water and ETH can also occur. The possibility of the significant contribution of the O−H···O hydrogen bonds between ETH and water can be ruled out as it appears around 3400 cm^{-1}. Hence, the enhanced intensity of the IR peak at 3200 cm^{-1} is dominant because of the increased aggregation of water molecules via the strong $O-H_w\cdots O_w$ hydrogen bonds. In contrast to the ETH−water mixture, the intensity of the peak around 3370 cm^{-1} is more than that of the peak at 3200 cm^{-1}

DOI: 10.1021/acs.jpcb.8b04365
J. Phys. Chem. B 2018, 122, 6616−6626

as compared to the bulk water along with the appearance of a peak at the high-frequency region of ∼3670 cm^{-1} whose intensity increases with the increase of TFE (Figure 1b, clearly shown in second plot of Figure 1c) in the water-rich region of the aqueous mixture of TFE. The appearance of a high-frequency peak at ∼3670 cm^{-1} and its increase in the intensity with the addition of TFE (blue square region in the Figure 1b) indicates that it originates probably from the weak interaction between water and TFE; hence, we tentatively assign it to the $O-H_w\cdots F_{TFE}$ interaction between the OH group of water and the fluorine of TFE. Indeed, lipid as well as air/water interfaces also have shown an IR feature at 3640 cm^{-1} which has been attributed to water interacting with the hydrophobic regions of the interfaces.[37,39] The decrease in the intensity of the peak around 3200 cm^{-1} indicates that the clustering of water decreases on the addition of TFE in the aqueous mixture. The decrease in the water clustering is due to the hydrogen bonding between water and TFE via the $O-H_w\cdots O_{TFE}$ and $O-H_w\cdots F_{TFE}$ interactions which in turn increases the intensity of the IR peaks at ∼3370 and 3660 cm^{-1}. The spectral change in the IR spectra of the aqueous mixtures of alcohols indicates that even a small amount of hydrophobic $-CF_3$ group of TFE plays an important role in the reorganization of the hydrogen bond network of the TFE−water mixture.

In the intermediate region of the ETH−water mixture, the intensity of the peak at ∼3370 cm^{-1} is either equal or more than the intensity of the peak at 3200 cm^{-1}, and the center of the peak position gets blue-shifted. The change in the spectral shape as well as the peak position indicates that the average hydrogen bond strength of the mixture in the intermediate region decreases when compared to that of pure water as well as the water-rich region, which is due to the fact that the contribution of the ETH−water hydrogen bond outweighs the effect of the hydrogen bonding between water molecules (clearly shown in the first plot of Figure 1d). In the intermediate region of the TFE−water mixture, the center of the peak position of the IR spectra of the mixture is blue-shifted, and the amount of the blue shift is more than that of the ETH−water mixture; the intensity of the peak at 3370 cm^{-1} is more compared to the peak at 3200 cm^{-1} along with a more intense and broad IR feature at ∼3650 cm^{-1} as compared to the water-rich region of the same mixture (depicted in the second plot of Figure 1d). The higher blue shift in the center of the peak position of the IR spectra of the TFE−water than that of the ETH−water mixture indicates that the average hydrogen bond strength of water molecules becomes more weak in the case of TFE as compared to ETH in their aqueous mixtures. The increase in the intensity of the peak at 3650 cm^{-1} suggests that a significant number of water molecules orient around the $-CF_3$ terminal and interact through the $O-H_w\cdots F_{TFE}$ interaction which probably breaks the hydrogen bond between water molecules as well as cooperates in the formation of stronger $O-H_{w/TFE}\cdots O_{TFE/w}$ hydrogen bonds between water and the TFE molecules, resulting in an increased blue shift in its IR spectra than that of ETH.

In the alcohol-rich region of the aqueous mixture of ETH, we get a single-peak IR feature around 3330 cm^{-1}, suggesting that the contributions from the self-aggregated ETH molecules via $O-H_{ETH}\cdots O_{ETH}$ dominate over the contributions from the hydrogen bonds between water molecules as well as that between water and ETH molecules. In the case of the TFE−water mixture, two band features of the mixture converge to one band at 3340 cm^{-1}, and the intensity of the band at 3670 cm^{-1} decreases with the appearance of a new peak around 3630 cm^{-1} (brown square area in Figure 1b) whose intensity increases with the increase of TFE, clearly indicating that the contribution of the self-aggregated TFE molecules through the $O-H_{TFE}\cdots F_{TFE}$ and $O-H_{TFE}\cdots O_{TFE}$ interactions prevails over the hydrogen bonds between water molecules as well as that between water and TFE molecules.

To quantify the population of different hydrogen-bonded species such as alcohol−alcohol, water−water, and alcohol−water in the aqueous mixture of alcohol, the IR spectra of the water mixture of alcohol have been deconvoluted by applying the method proposed by Ratajska-Gadomska and Gadomski (Figures S2 and S3).[50] Five Gaussian peaks centered at 3080, 3200, 3400, 3500, and 3600 cm^{-1} have been used for the deconvolution of the IR spectrum of bulk water. The peak at 3080 cm^{-1} has been assigned to the Fermi resonance arising from the bending mode (1630 cm^{-1}) and the stretching mode (3200 cm^{-1}) of the water molecules. The peak around 3200 cm^{-1} has been assigned to the water molecules organized in the symmetrical tetrahedral environment, whereas the peak at 3400 cm^{-1} has been attributed to the asymmetric tetrahedral hydrogen-bonded network. The peaks at 3500 and 3600 cm^{-1} have been designated to the weakly hydrogen-bonded species. Two Gaussian peaks centered at ∼3280 and 3360 cm^{-1} representing the different sizes of the clusters of ETH have been used to deconvolute the IR spectra of ETH. Table 1 depicts the normalized contribution of different peaks, and the normalization has been done by the total area of the peaks which is the sum of the areas of five water peaks and two ETH peaks. It can be seen that the population of the peak at 3200 cm^{-1} increases, and simultaneously the contribution of the peaks at 3500 and 3600 cm^{-1} decreases in the water-rich region of the aqueous mixture of ETH. The deconvoluted data suggest an increase in the contribution of the tetrahedral water network as compared to the bulk water at the cost of the weakening of the asymmetrical hydrogen-bonded network of water molecules in the water-rich region of the aqueous mixture of ETH. In the intermediate region, the population of the water peak at 3200 cm^{-1} decreases, and the contribution of the peaks at 3500 and 3600 cm^{-1} increases, indicating that the tetrahedral arrangement of water molecules gets loosened and the population of the water molecules in the asymmetrical tetrahedral hydrogen bond network increases. Apart from this, the contribution of the ETH peak increases in the intermediate region of the mixture which could be either because of the water−ETH hydrogen bonding or self-clustering of the ETH molecules. However, in the intermediate region, it is expected that the contribution of the water−ETH hydrogen bonding should dominate the clustering of the ETH molecules. The deconvoluted data of the water mixture of ETH in the intermediate region suggest that the tetrahedral structure of water is broken/loosened, which forms hydrogen bonds with the ETH molecules. In fact, the excess compressibility of the water mixture of ETH increases sharply in the intermediate region, which is attributed to the decrease in the tetrahedral hydrogen bond network.

In contrast to ETH, because of the $O-H_w\cdots F_{TFE}$ interaction, an additional peak at ∼3650 cm^{-1} has been used to deconvolute the IR spectra of the aqueous mixture of TFE. Unlike the ETH−water mixture, the intensity ratio of the water peaks at 3200 and 3400 cm^{-1} decreases along with an increase in the population of the peak at the high-frequency region at ∼3650 cm^{-1} in the water-rich region of the aqueous mixture of

DOI: 10.1021/acs.jpcb.8b04365
J. Phys. Chem. B 2018, 122, 6616−6626

Table 1. Population of the Different Hydrogen-Bonded Species in the Different Compositions of the Water Mixtures of ETH and TFE Obtained from the Deconvolution of IR Lines

	ETH···water					
	water					
X_w	3050	3200	3400	3500	3600	ETH
1.00	0.091	0.450	0.314	0.127	0.018	
0.97	0.089	0.462	0.305	0.073	0.044	0.027
0.93	0.073	0.464	0.304	0.061	0.027	0.073
0.88	0.088	0.452	0.297	0.062	0.024	0.077
0.83	0.087	0.437	0.288	0.087	0.020	0.082
0.76	0.100	0.395	0.265	0.080	0.019	0.132
0.68	0.063	0.364	0.239	0.115	0.026	0.190
0.58	0.064	0.320	0.203	0.136	0.030	0.247
0.45	0.082	0.263	0.158	0.136	0.027	0.334
0.36	0.080	0.234	0.145	0.125	0.020	0.396
0.27	0.084	0.222	0.142	0.123	0.024	0.406
0.17	0.072	0.157	0.096	0.112	0.019	0.545
0.12	0.069	0.072	0.047	0.072	0.008	0.733
0.03	0.054	0.027	0.034	0.033	0.010	0.842
	TFE···water						
	water						
X_w	3050	3200	3400	3500	3600	TFE	TFE···W
0.97	0.082	0.444	0.329	0.072	0.024	0.047	0.002
0.94	0.076	0.422	0.331	0.069	0.025	0.073	0.003
0.90	0.065	0.403	0.335	0.067	0.033	0.092	0.003
0.86	0.065	0.393	0.335	0.060	0.040	0.103	0.004
0.80	0.064	0.385	0.332	0.074	0.039	0.104	0.005
0.73	0.068	0.369	0.288	0.084	0.047	0.144	0.007
0.63	0.067	0.295	0.209	0.142	0.030	0.244	0.007
0.57	0.069	0.255	0.173	0.119	0.034	0.342	0.008
0.50	0.069	0.235	0.158	0.112	0.029	0.376	0.021
0.31	0.067	0.211	0.146	0.117	0.030	0.408	0.021
0.28	0.069	0.196	0.144	0.110	0.047	0.415	0.019
0.20	0.051	0.123	0.115	0.051	0.033	0.602	0.024
0.15	0.022	0.093	0.078	0.016	0.010	0.773	0.008
0.12	0.008	0.078	0.054	0.014	0.008	0.830	0.007
0.08	0.013	0.035	0.031	0.013	0.008	0.893	0.007
0.04	0.013	0.032	0.013	0.015	0.011	0.911	0.006

TFE. Noticeably, an increase in the contribution of the TFE part in the water-rich region is more than that of ETH in its water mixture, indicating that the contribution of the water−TFE hydrogen bond is more significant. The deconvoluted data of the TFE−water mixture in the water-rich region evoke that the tetrahedral hydrogen-bonded structure of water is broken/loosened and it realizes more of the asymmetric hydrogen-bonded environment because of the hydrogen bonding of water with the TFE clusters via $O-H_{w/TFE}\cdots O_{TFE/w}$ and $O-H_w\cdots F_{TFE}$ interactions.

3.2. MD Simulations. The deconvoluted IR data describe the difference in the hydrogen bond structure between the aqueous mixtures of ETH and TFE; however, the mode of interaction between water and alcohol, for example, whether water is a donor to alcohol or vice versa is not evident. Hence, we have performed MD simulations using all-atom OPLS and Amber99sb-ildn force fields for different compositions of the aqueous mixtures of ETH and TFE to enhance the depth of understanding about the mode of interaction between the different molecules of the mixtures. The results obtained from the OPLS force field are shown in the main text (Figures 2−4), whereas the comparisons of the results of both the force fields are shown in the Supporting Information (Figures S4−S8).

To understand the self-aggregation of water and alcohol in their respective mixtures, $g(r)$ between oxygen and alcohol have been calculated as depicted in Figures 2 and S4. It can be seen that the intensity of the first peak of $g(r)$ between hydrogen and oxygen of ETH decreases with the increase of water, suggesting that the aggregation of ETH via the $O-H_{ETH}\cdots O_{ETH}$ hydrogen bond decreases with the increase of water. However, the intensity of the first peak of $g(r)$ between the hydrogen and oxygen of water increases with the increase of ETH, indicating the aggregation of water via the $O-H_w\cdots O_w$ hydrogen bond enhances with the addition of ETH in its aqueous mixture. The trend of the $g(r)$ data obtained from the Amber99sb-ildn force field is similar to that of the OPLS force field; however, the aggregation of water in the ETH-rich region is higher as compared to that of the OPLS force field.

Similar to the ETH−water case, the $g(r)$ between the hydrogen and oxygen of TFE (Figures 2c and S5a,b) obtained from both the force fields decreases with the increase of water in the TFE−water case; however, the amount of decrease is slightly higher than that of the ETH−water mixture, pointing that the aggregation of TFE via $O-H_{TFE}\cdots O_{TFE}$ is less than that of ETH in their aqueous mixtures. To understand this, the $g(r)$ between the fluorine and hydrogen of OH of TFE has been calculated using both the force fields (depicted in Figures 2d and S6a,b), and it is observed that the intensity of the first peak of $g(r)$ increases and is shifted slightly toward a lower distance for a higher mole fraction of water in the mixture, indicating that the $O-H_{TFE}\cdots F_{TFE}$ interaction between the TFE molecules gets stronger and prominent with the increment of water in their mixtures. The $O-H_{TFE}\cdots F_{TFE}$ interaction between the TFE molecules causes more of a decrease in the number of $O-H_{TFE}\cdots O_{TFE}$ hydrogen bonds than the ETH on the addition of water in their respective mixtures. In contrast to the aqueous mixture of ETH, the aggregation of water via the $O-H_w\cdots O_w$ hydrogen bond does not increase monotonically with the increase of TFE in their aqueous mixture (Figures 2e and S5c,d). The nonmonotonic nature has been obtained from both the force fields; however, the point of nonmonotonicity is different for both force fields. The intensity of the first peak of $g(r)$ between the hydrogen and oxygen of water obtained from the OPLS force field increases up to $X_w \approx 0.30$, and after that it decreases, whereas nonmonotonicity appears at $X_w \approx 0.50$ for the Amber99sb-ildn force field. Although nonmonotonicity has been observed in both the force fields, however, the decrease in $g(r)$ is more prominent in the case of the Amber99sb-ildn force field. The nonmonotonic nature of water clustering with the increase of TFE in their mixture is probably because of the enhanced heterogeneity of the hydrogen bonding between the water and TFE molecules than that of the ETH case as TFE can interact with water via the OH as well as $-CF_3$ groups.

Hence, the $g(r)$ plots between the hydrogen of the OH of alcohol and oxygen of water and vice versa have been calculated using both the force fields (depicted in Figures 3, S7, and S8) to explore the intermolecular hydrogen bonding between the different sites of alcohol and water. From the $g(r)$ plots, it is evident that ETH is predominantly a hydrogen bond donor and that it interacts with water via the $O-H_{ETH}\cdots O_w$ hydrogen bond as the intensity of the first peak of $g(r)$ between the hydrogen of the OH of ETH and oxygen of water (Figures 3a and S7a,b) is higher than the $g(r)$ between the hydrogen of the

DOI: 10.1021/acs.jpcb.8b04365
J. Phys. Chem. B 2018, 122, 6616−6626

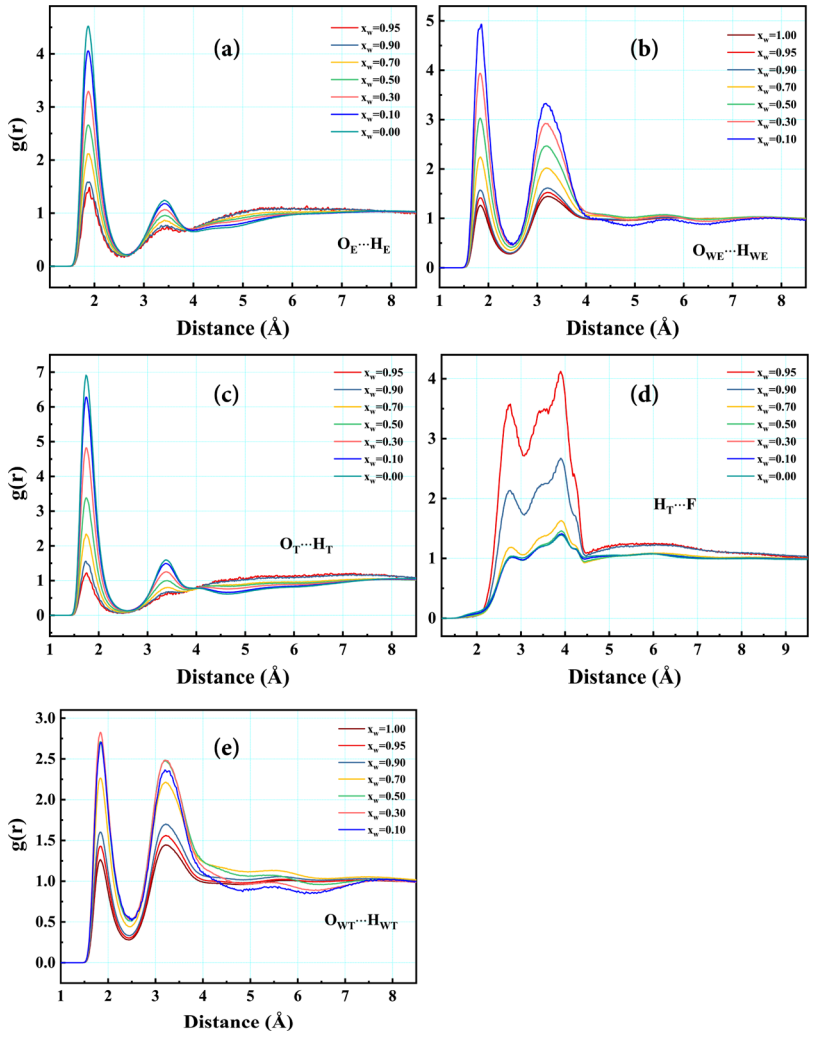

Figure 2. $g(r)$ plots between the oxygen and hydrogen of ETH (a) and water (b) for different compositions of the aqueous mixture of ETH. (c) $g(r)$ plot for oxygen and hydrogen of TFE; (d) $g(r)$ plot between the hydrogen and fluorine of TFE; and (e) $g(r)$ plot for the oxygen and hydrogen of water for different compositions of the aqueous mixture of TFE. The simulations have been performed using the OPLS all-atom force field.

OH of water and oxygen of alcohol (Figures 3b and S7c,d) for any composition. Similarly, TFE acts predominantly as a hydrogen bond donor and interacts with water via the O−$H_{TFE}\cdots O_w$ hydrogen bond in the aqueous mixture of TFE, as shown in the $g(r)$ plots between the hydrogen of the OH of TFE and oxygen of water and vice versa (Figures 4c,d and S8a−d). However, the hydrogen bond donor capability of the OH of TFE toward the oxygen of water via O−$H_{TFE}\cdots O_w$ is increased in their aqueous mixture as compared to the ETH−water mixture, which is evident from the increased intensity (∼2-fold) of the $g(r)$ between the hydrogen of the OH of alcohol and oxygen of water for the TFE−water mixture than that for the ETH−water mixture. Simultaneously, the hydrogen bond donor capability of water toward TFE via O−$H_w\cdots O_{TFE}$ in their aqueous mixture has decreased as compared to the ETH−water mixture as the $g(r)$ between the hydrogen of the OH of water and oxygen of alcohol of the TFE−water mixture is ∼1.5 times less than that of the ETH−water mixture.

Further, to understand the origin of the enhanced hydrogen bond donor capability of TFE compared to ETH in their water mixtures, we investigated the interaction of water with the $-CF_3$ group of TFE by calculating the $g(r)$ between the fluorine of the $-CF_3$ terminal of TFE and the hydrogen of the OH group of water using both force fields (shown in Figures 3e and S6c,d). It can be seen that the $g(r)$ between the fluorine terminal of $-CF_3$ and the hydrogen of the OH group of water shows a peak within 3.5 Å, indicating the presence of an extremely weak O−$H_w\cdots F_{TFE}$ interaction in the water mixture of TFE. The O−$H_w\cdots F_{TFE}$ interaction enhances with the increment of TFE in their water mixture as shown by the $g(r)$ plots of Figure 3e. The increase of the O−$H_w\cdots F_{TFE}$ interaction causes the switching of the water-binding site from the OH to the $-CF_3$ terminal of TFE and hence reduces the probability of the formation of the O−$H_w\cdots O_{TFE}$ hydrogen bond more rapidly compared to ETH, as discussed above and shown in Figure 3b,d. Moreover, because of the O−$H_w\cdots F_{TFE}$ interaction, the oxygen of water is easily approachable for the O−$H_{TFE}\cdots O_w$ hydrogen bond probably through the cyclic structure having both O−$H_{TFE}\cdots O_w$ as well as O−$H_w\cdots F_{TFE}$ interactions (Figure 3f), causing an increase in the intensity of the first peak of $g(r)$ between the hydrogen of the OH of alcohol and oxygen of water for the aqueous mixture of TFE than that of ETH (Figure 3a,c).

Indeed, in the supersonic jet conditions, a cyclic complex of water with TFE having O−H···F and O−H···O contacts was observed.[51,52] Furthermore, the O−$H_w\cdots F_{TFE}$ interaction

DOI: 10.1021/acs.jpcb.8b04365
J. Phys. Chem. B 2018, 122, 6616−6626

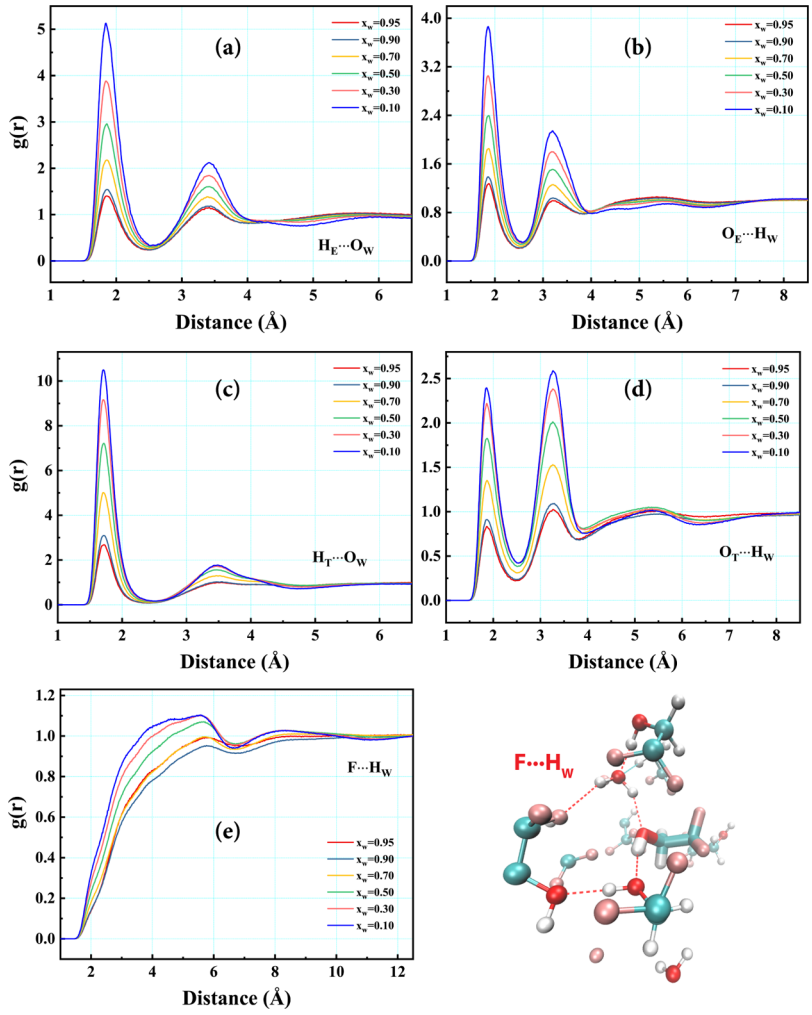

Figure 3. (a,b) $g(r)$ plots between the hydrogen of ETH and oxygen of water as well as the hydrogen of water and oxygen of ETH, respectively, for different mole fractions of the water mixture of ETH; (c,d) $g(r)$ plots between the hydrogen of TFE and oxygen of water as well as the hydrogen of water and oxygen of TFE, respectively; (e) $g(r)$ plot between the hydrogen of water and fluorine of TFE for different compositions of the TFE–water mixture. (f) Snapshot of the TFE–water mixture having $O-H_w\cdots F_{TFE}$ and $O-H_{TFE}\cdots O_w$ contacts. The simulations have been performed using the OPLS all-atom force field.

reduces the aggregation of water molecules through the $O-H_w\cdots O_w$ hydrogen bond as the $O-H_w\cdots F_{TFE}$ and $O-H_{TFE}\cdots O_w$ interactions block the hydrogen- and oxygen-binding sites of water for hydrogen bonding with another water molecule.

Further, the coordination number (CN) for the different interactions between alcohol and water molecules has been computed, as represented in Figure 4. The CN data depict that self-aggregation of alcohol and water molecules is more prominent in ETH than that in TFE in their water mixtures (Figure 4a,b). It also indicates that the OH group of TFE is a strong hydrogen bond donor than that of ETH in their aqueous mixtures as the CN number for the $O-H_w\cdots O_{alc}$ interaction is higher for the aqueous mixture of ETH than that of TFE, whereas the CN number for the $O-H_{alc}\cdots O_w$ interaction is higher for TFE than that for ETH in their aqueous mixture (Figure 4c,d). The CN for the $O-H_{TFE}\cdots F_{TFE}$ interaction decreases and simultaneously, the CN for the $O-H_w\cdots F_{TFE}$ interaction increases (Figure 4e) with the increment of water content, indicating that the addition of water decreases the $O-H_{TFE}\cdots F_{TFE}$ interaction between TFE molecules by increasing its interaction with the TFE molecules via $O-H_w\cdots F_{TFE}$ interactions. The CN data suggest that the increased $O-H_w\cdots F_{TFE}$ interaction cooperates to increase the hydrogen bond donor capability of the OH group, which is in good agreement with the results obtained from the radial distribution calculations.

3.3. Quantum Chemical Calculation. MD simulation renders the probability of interactions as well as the solvent organization of any system; however, it lacks the information about the kind of interactions as well as their inherent nature. To understand the nature of different interactions involved in the water mixtures of alcohol and to correlate the experimental IR data with the MD simulation results, we performed the AIM analysis and frequency calculations on the structures obtained from the MD simulations within 5.0 Å (the cutoff of 5.0 Å has been chosen as it describes the first solvation shell of alcohols). Figure 5 shows the molecular graph of the electron densities at different (3, −1) bond critical points (BCPs) of the aqueous mixtures of ETH and TFE in two different concentrations. Further, we calculated the electron density (ρ) and Laplacian (L) at each BCP to understand the nature of the interaction between two interacting atoms. It is important to mention that only those BCPs whose ρ and L are higher than 0.002 and 0.02 au, respectively, have been considered as they confirm the

DOI: 10.1021/acs.jpcb.8b04365
J. Phys. Chem. B 2018, 122, 6616–6626

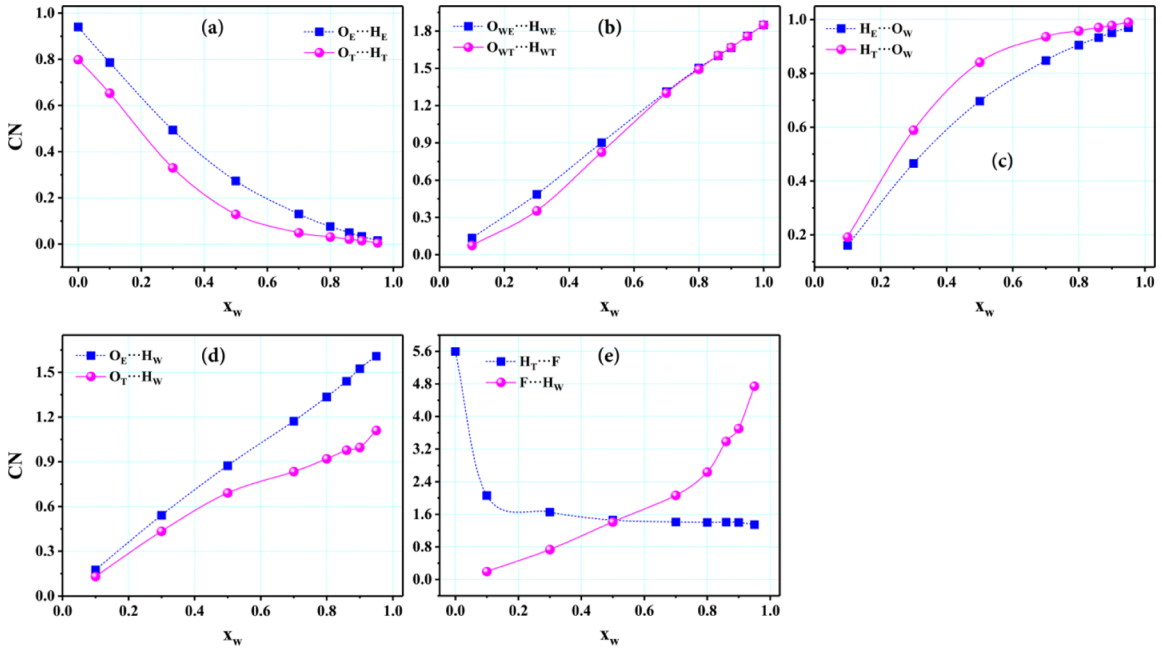

Figure 4. CN for different modes of interactions of the water mixture of ETH and TFE.

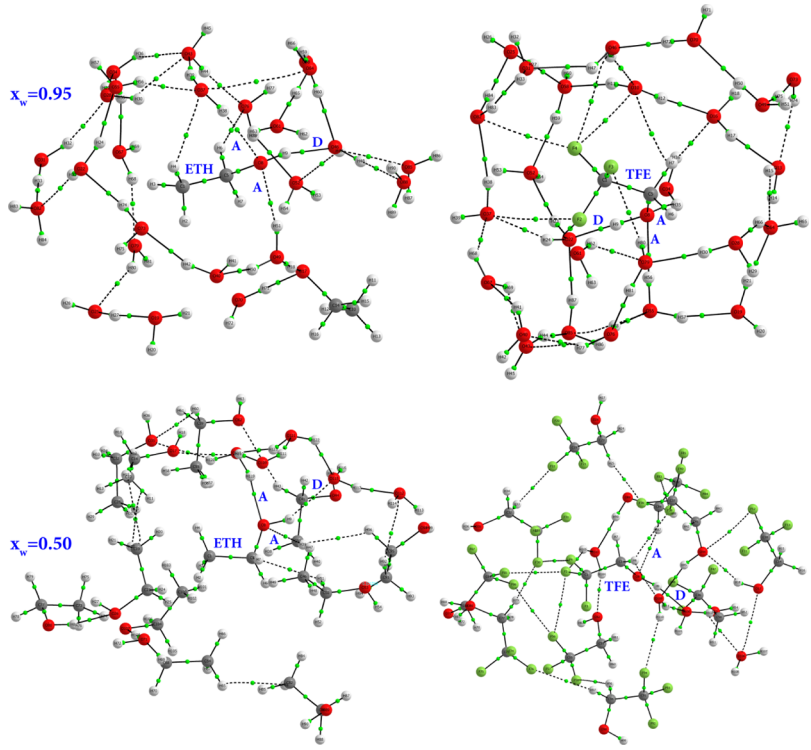

Figure 5. Molecular graph obtained from the AIM calculation of the aqueous mixture of ETH and TFE for two different mole fractions, X_w = 0.95 and X_w = 0.50, respectively. The green dots show the presence of (3, −1) BCP. The (3, +1), and (3, +3) BCPs representing the ring and cage structures have not been shown for clarity of visualization. Only those BCPs have been shown whose ρ and Laplacian L values are higher than 0.002 and 0.02 au, respectively as they confirm the existence of the noncovalent interaction.

existence of the noncovalent interactions. In the water-rich region of the water mixtures of ETH and TFE, clusterization of water takes place around alcohols. In both cases, the hydrogen of the OH group of alcohol is hydrogen-bonded to water (denoted as D), whereas the oxygen of alcohol works as an acceptor and forms two hydrogen bonds with the hydrogen of water molecule (denoted as A). However, in the case of TFE, a significant number of BCPs have been found between the fluorine terminals of TFE and water which confirms the presence of $O-H_w\cdots F_{TFE}$ interaction. It can also be seen that the orientation of water toward the $-CF_3$ terminal of TFE has changed because of the $O-H_w\cdots F_{TFE}$ interactions as compared to the orientation of water around the OH group of TFE and ETH. Moreover, the $O-H_w\cdots F_{TFE}$ interaction causes an

DOI: 10.1021/acs.jpcb.8b04365
J. Phys. Chem. B 2018, 122, 6616−6626

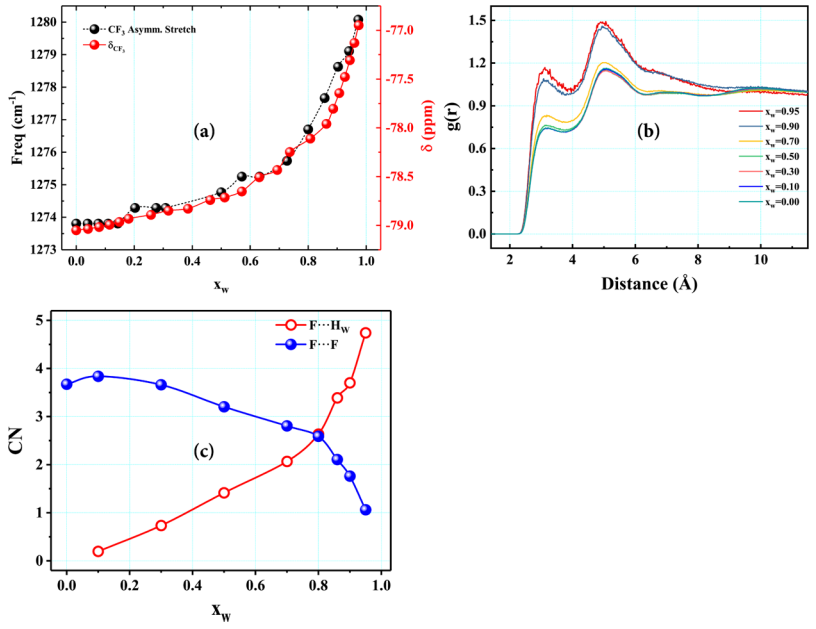

Figure 6. (a) Change in the C−F stretching frequency (black) as well as ^{19}F NMR (red). (b) Change in $g(r)$ for the F···F interaction. (c) Change in the CN for the F···F (blue) and F···H_w interactions for the different mole fractions of the water mixture of TFE.

increase in the population of asymmetric hydrogen-bonded water molecules. The electron density of the donor hydrogen of alcohol and oxygen of water (D) is 0.05 au for the ETH case, whereas its value for TFE is 0.07 au. The increased electron density for D shows that TFE is a stronger hydrogen bond donor than ETH in their water mixture and that the strong donor capability of TFE is correlated with the O−H_w···F_{TFE} interaction which is in line with the experimental as well as MD simulation results. On increasing the alcohol concentration, water gets squeezed out mostly from the first hydration shell of the alcohol, and alcohol prefers to self-clusterize, as shown in Figure 5. However, the clusterization of TFE is different from that of ETH as TFE aggregates through the F_{TFE}···F_{TFE} interaction along with the O−H_{TFE}···O_{TFE} hydrogen bonds.

The calculated IR data (for the structures obtained from the MD simulation within 5.0 Å) for the alcohol−water mixtures show the appearance of complex features because of the large number of molecules (Figure S9). However, it is clear that the vibrational feature for the O−H_w···F_{TFE} interactions appears above 3600 cm^{-1}, whereas the O−$H_{alc/w}$···$O_{w/alc}$ interactions show the feature appearing below 3600 cm^{-1}. To assert the frequency data, we calculated the optimized structures and frequency of the small-sized clusters of ETH and TFE with water molecules in their aqueous medium. We have found that a significant number of O−H_w···F_{TFE} interactions are present for the TFE−water clusters bigger than the dimer along with the O−H_{TFE}···O_w interaction, whereas only the O−H_{ETH}···O_w interaction exists for the ETH−water clusters (Figure S10). The calculated IR data for the ETH−water cluster depict that the vibrational feature for the OH of water interacting with alcohol appears around ∼3400 cm^{-1}, whereas the alcohol OH interacting with water shows the feature at ∼3450 cm^{-1} (Table S16). The IR band position of water depends on the cluster size, and it gets red-shifted with the increase of the cluster size. The IR frequency calculation of ETH−water clusters asserts that the enhanced aggregation of water molecules in the ETH−water mixture causes an increase in the intensity of the IR peak at ∼3200 cm^{-1} in the water-rich region, which is in line with the MD simulation results. The O−H stretching for the O−H_w···F_{TFE} hydrogen-bonded system of the TFE−water cluster appears at ∼3634 cm^{-1}, which is in accordance with the experimental IR data observed at ∼3640 cm^{-1}, assuring the presence of O−H_w···F_{TFE}-interacted species, as predicted from the experimental as well as MD simulation studies. The simultaneous increase of the experimental IR peaks at ∼3400 cm^{-1} as well as at ∼3640 cm^{-1} clearly points that the O−H_w···F_{TFE} cooperates in the formation of strong O−H_{TFE}···O_w hydrogen bonds in accordance with the MD simulation data.

3.4. Role of −CF_3 Group in Hydrogen Bond Network.

The C−F stretching and ^{19}F NMR of the CF_3 group of TFE for the different compositions of water have been measured (as shown in Figures 6a and S11) to assert the role of the −CF_3 group in the hydrogen bond network of the water mixture of TFE. It can be found that the C−F stretching frequency gets red-shifted, and simultaneously a downfield shift of ^{19}F NMR was observed with the increment of TFE in its water mixture. The change in the C−F vibration frequency as well as ^{19}F NMR shows a bimodal nature, where the change is sharp till $X_w \approx 0.7$ and very slow for $X_w < 0.7$. The fluorine group of TFE interacts with water via the O−H_w···F_{TFE} interaction, whereas in the alcohol-rich region they interact with the other fluorine via the F_{TFE}···F_{TFE} interaction, as also shown in the AIM calculation. Hence, we have calculated the $g(r)$ as well as CN for the F_{TFE}···F_{TFE} interaction and compared them with the O−H_w···F_{TFE} interaction for the different mole fractions of the water mixture of TFE (Figure 6b,c). It can be seen from the $g(r)$ calculation that the extent of F_{TFE}···F_{TFE} interaction increases with the increment of TFE in its water mixture. The CN of the O−H_w···F_{TFE} interaction decreases sharply till $X_w \approx 0.7$; after that, the extent of decrease of the CN is less. In contrast, the CN for the F_{TFE}···F_{TFE} interaction increases sharply till $X_w \approx 0.7$, and then the increase is very less. The CN data suggests that the sharp change observed in the IR and NMR in the range of $X_w \approx 0.7$ is mainly because of the O−H_w···F_{TFE} interaction, whereas the flat change after $X_w < 0.7$ is the cumulative effect of the O−H_w···F_{TFE} and F_{TFE}···F_{TFE} interactions. The NMR, IR, and CN data

DOI: 10.1021/acs.jpcb.8b04365
J. Phys. Chem. B 2018, 122, 6616−6626

for fluorine confirm that fluorine makes $O-H_w\cdots F_{TFE}$ hydrogen bond with water molecules causing a change in the orientation of water as well as the hydrogen-bonding site, which in turn increases the hydrogen bond donor capability of the OH group of TFE as well as decreases the aggregation of water in its aqueous mixture.

4. CONCLUSION

The deconvolution of the IR lines in the OH-stretching region, MD simulation, and quantum chemical calculations have been utilized to decode the hydrogen bond network of the water mixtures of ETH and TFE. In the water rich region of the aqueous mixture of ETH, water clustering via $O-H_w\cdots O_w$ interaction dominates over water-ETH hydrogen bonds. However, with further addition of ETH in their mixture, the contribution of the $O-H_{ETH}\cdots O_w$ hydrogen bonds between ETH and water outweighs the contribution of water clustering. In the case of an aqueous mixture of TFE, water changes its binding site from the hydrophilic OH to the hydrophobic $-CF_3$ terminal and interacts with the $-CF_3$ group of TFE via the $O-H_w\cdots F_{TFE}$ interaction. The $O-H_w\cdots F_{TFE}$ interaction causes an increase in the $O-H_{TFE}\cdots O_w$ hydrogen bonds through the cooperativity effect as well as lessens the clustering of water via the $O-H_w\cdots O_w$ interaction as compared to the water mixture of ETH. In the TFE-rich region, the fluorine of TFE interacts among themselves through fluorous interaction which maximizes the $O-H_{TFE}\cdots O_{TFE}$ interactions. This study describes that the hydrophobic $-CF_3$ group of TFE plays an important role in the reorganization of the hydrogen bond network of the aqueous mixture of TFE which probably makes them useful for the chemical as well as medicinal applications.

■ ASSOCIATED CONTENT

Supporting Information

The Supporting Information is available free of charge on the ACS Publications website at DOI: 10.1021/acs.jpcb.8b04365.

Volumetric and thermodynamic quantities of the water mixture of ETH and TFE calculated from the MD simulations as well as their comparison with the experimental as well as other simulation data; detailed description of the deconvolution of the IR lines; simulated IR spectrum; and AIM analysis of the different sizes of alcohol clusters (PDF)

■ AUTHOR INFORMATION

Corresponding Author

*E-mail: sppcs@iacs.res.in.

ORCID

Saptarsi Mondal: 0000-0003-1140-9322

Biswajit Biswas: 0000-0002-9075-1689

Prashant Chandra Singh: 0000-0001-9357-9039

Notes

The authors declare no competing financial interest.

■ ACKNOWLEDGMENTS

The Council of Scientific and Industrial Research (CSIR) [grant no. 01 (2803)/14/EMR-II] as well as Department of Science and Technology (DST-SERB) [grant no. EMR/2015/001605], India supported this work. S. M. and B. B. thank the institute and CSIR, respectively, for their fellowships.

■ REFERENCES

(1) Takamuku, T.; Tanaka, M.; Sako, T.; Shimomura, T.; Fujii, K.; Kanzaki, R.; Takeuchi, M. Solvation of the Amphiphilic Diol Molecule in Aliphatic Alcohol−Water and Fluorinated Alcohol−Water Solutions. *J. Phys. Chem. B* **2010**, *114*, 4252−4260.

(2) Schuh, M. D.; Baldwin, M. C. α-Helix Formation in Melittin and β-Lactoglobulin A Induced by Fluorinated Dialcohols. *J. Phys. Chem. B* **2006**, *110*, 10903−10909.

(3) Fioroni, M.; Diaz, M. D.; Burger, K.; Berger, S. Solvation Phenomena of a Tetrapeptide in Water/Trifluoroethanol and Water/Ethanol Mixtures: A Diffusion NMR, Intermolecular NOE, and Molecular Dynamics Study. *J. Am. Chem. Soc.* **2002**, *124*, 7737−7744.

(4) Clot, E.; Eisenstein, O.; Jasim, N.; Macgregor, S. A.; McGrady, J. E.; Perutz, R. N. C−F and C−H Bond Activation of Fluorobenzenes and Fluoropyridines at Transition Metal Centers: How Fluorine Tips the Scales. *Acc. Chem. Res.* **2011**, *44*, 333−348.

(5) Liao, K.-C.; Bowers, C. M.; Yoon, H. J.; Whitesides, G. M. Fluorination, and Tunneling across Molecular Junctions. *J. Am. Chem. Soc.* **2015**, *137*, 3852−3858.

(6) Khan, M. V.; Rabbani, G.; Ahmad, E.; Khan, R. H. Fluoroalcohols-induced modulation and amyloid formation in conalbumin. *Int. J. Biol. Macromol.* **2014**, *70*, 606−614.

(7) Böhm, H.-J.; Banner, D.; Bendels, S.; Kansy, M.; Kuhn, B.; Müller, K.; Obst-Sander, U.; Stahl, M. Fluorine in Medicinal Chemistry. *ChemBioChem* **2004**, *5*, 637−643.

(8) Müller, K.; Faeh, C.; Diederich, F. Fluorine in Pharmaceuticals: Looking Beyond Intuition. *Science* **2007**, *317*, 1881−1886.

(9) Narita, T. Synthesis of novel fluorinated polymers: facile carbon-carbon bond formation aided by fluorine substituents. *Polym. J.* **2011**, *43*, 497−515.

(10) Matsumoto, K.; Kubota, M.; Matsuoka, H.; Yamaoka, H. Water-Soluble Fluorine-Containing Amphiphilic Block Copolymer: Synthesis and Aggregation Behavior in Aqueous Solution. *Macromolecules* **1999**, *32*, 7122−7127.

(11) Castagnola, M.; Cassiano, L.; Messana, I.; Paci, M.; Rossetti, D. V.; Giardina, B. Effect of 2,2,2-trifluoroethanol on capillary zone electrophoretic peptide separations. *J. Chromatogr. A* **1996**, *735*, 271−281.

(12) Shao, Q. The addition of 2,2,2-trifluoroethanol prevents the aggregation of guanidinium around protein and impairs its denaturation ability: A molecular dynamics simulation study. *Proteins* **2014**, *82*, 944−953.

(13) Culik, R. M.; Abaskharon, R. M.; Pazos, I. M.; Gai, F. Experimental Validation of the Role of Trifluoroethanol as a Nanocrowder. *J. Phys. Chem. B* **2014**, *118*, 11455−11461.

(14) Jalili, S.; Akhavan, M. A Molecular Dynamics Simulation Study of Conformational Changes and Solvation of Aβ Peptide in Trifluoroethanol and Water. *J. Chem. Theory Comput.* **2009**, *08*, 215−231.

(15) Roccatano, D.; Colombo, G.; Fioroni, M.; Mark, A. E. Mechanism by which 2,2,2-trifluoroethanol/water mixtures stabilize secondary-structure formation in peptides: A molecular dynamics study. *Proc. Natl. Acad. Sci. U.S.A.* **2002**, *99*, 12179−12184.

(16) Gast, K.; Zirwer, D.; Müller-Frohne, M.; Damaschun, G. Trifluoroethanol-induced conformational transitions of proteins: Insights gained from the differences between α-lactalbumin and ribonuclease A. *Protein Sci.* **1999**, *8*, 625−634.

(17) Jalili, S.; Akhavan, M. Molecular dynamics simulation study of association in trifluoroethanol/water mixtures. *J. Comput. Chem.* **2010**, *31*, 286−294.

(18) Gottler, L. M.; de la Salud-Bea, R.; Marsh, E. N. G. The Fluorous Effect in Proteins: Properties of α4F6, a 4-α-Helix Bundle Protein with a Fluorocarbon Core. *Biochemistry* **2008**, *47*, 4484−4490.

(19) Lee, K.-H.; Lee, H.-Y.; Slutsky, M. M.; Anderson, J. T.; Marsh, E. N. G. Fluorous Effect in Proteins: De Novo Design and Characterization of a Four-α-Helix Bundle Protein Containing Hexafluoroleucine. *Biochemistry* **2004**, *43*, 16277−16284.

(20) Bilgiçer, B.; Fichera, A.; Kumar, K. A Coiled Coil with a Fluorous Core. *J. Am. Chem. Soc.* **2001**, *123*, 4393−4399.

DOI: 10.1021/acs.jpcb.8b04365
J. Phys. Chem. B 2018, 122, 6616−6626

(21) Neil, E.; Marsh, G. Towards the nonstick egg: designing fluorous proteins. *Chem. Biol.* **2000**, *7*, R153−R157.
(22) Luo, P.; Baldwin, R. L. Mechanism of Helix Induction by Trifluoroethanol: A Framework for Extrapolating the Helix-Forming Properties of Peptides from Trifluoroethanol/Water Mixtures Back to Water. *Biochemistry* **1997**, *36*, 8413−8421.
(23) Mondal, S.; Halder, R.; Biswas, B.; Jana, B.; Singh, P. C. Solvent organization around the perfluoro group of coumarin 153 governs its photophysical properties: An experimental and simulation study of coumarin dyes in ethanol as well as fluorinated ethanol solvents. *J. Chem. Phys.* **2016**, *144*, 184504.
(24) Mondal, S.; Chatterjee, S.; Halder, R.; Jana, B.; Singh, P. C. Role of Dispersive Fluorous Interaction in the Solvation Dynamics of the Perfluoro Group Containing Molecules. *J. Phys. Chem. B* **2017**, *121*, 7681−7688.
(25) Evans, M. E.; Burke, C. L.; Yaibuathes, S.; Clot, E.; Eisenstein, O.; Jones, W. D. Energetics of C−H Bond Activation of Fluorinated Aromatic Hydrocarbons Using a [Tp′Rh(CNneopentyl)] Complex. *J. Am. Chem. Soc.* **2009**, *131*, 13464−13473.
(26) Minamihonoki, T.; Ogawa, H.; Nomura, H.; Murakami, S. Thermodynamic properties of binary mixtures of 2,2,2-trifluoroethanol with water or alkanols at T=298.15 K. *Thermochim. Acta* **2007**, *459*, 80−86.
(27) Sassi, M.; Atik, Z. Excess molar volumes of binary mixtures of 2,2,2-trifluoroethanol with water, or acetone, or 1,4-difluorobenzene, or 4-fluorotoluene, or *α,α,α*, trifluorotoluene or 1-alcohols at a temperature of 298.15 K and pressure of 101 kPa. *J. Chem. Thermodyn.* **2003**, *35*, 1161−1169.
(28) Chitra, R.; Smith, P. E. A comparison of the properties of 2,2,2-trifluoroethanol and 2,2,2-trifluoroethanol/water mixtures using different force fields. *J. Chem. Phys.* **2001**, *115*, 5521−5530.
(29) Matsuo, S.; Yamamoto, R.; Tanaka, Y.; Kubota, H. Viscosity of mixtures of fluoroalcohols and water at high pressures. *Int. J. Thermophys.* **1993**, *14*, 835−849.
(30) Kaiser, B.; Laesecke, A.; Schmeck, M. Experimental study and correlation of the viscosity of 2,2,2-trifluoroethanol (TFE)-water mixtures. *Int. J. Thermophys.* **1989**, *10*, 713−726.
(31) Mondal, S.; Biswas, B.; Nandy, T.; Singh, P. C. Hydrophobic fluorine mediated switching of the hydrogen bonding site as well as orientation of water molecules in the aqueous mixture of monofluoroethanol: IR, molecular dynamics and quantum chemical studies. *Phys. Chem. Chem. Phys.* **2017**, *19*, 24667.
(32) Matsugami, M.; Yamamoto, R.; Kumai, T.; Tanaka, M.; Umecky, T.; Takamuku, T. Hydrogen bonding in ethanol−water and trifluoroethanol−water mixtures studied by NMR and molecular dynamics simulation. *J. Mol. Liq.* **2016**, *217*, 3−11.
(33) Bakó, I.; Radnai, T.; Funel, M. C. B. Investigation of structure of liquid 2,2,2 trifluoroethanol: Neutron diffraction, molecular dynamics, and ab initio quantum chemical study. *J. Chem. Phys.* **2004**, *121*, 12472.
(34) Harris, K. R.; Newitt, P. J.; Derlacki, Z. J. Alcohol tracer diffusion, density, NMR and FTIR studies of aqueous ethanol and 2,2,2-trifluoroethanol solutions at 25. *J. Chem. Soc., Faraday Trans.* **1998**, *94*, 1963−1970.
(35) Takamuku, T.; Kumai, T.; Yoshida, K.; Otomo, T.; Yamaguchi, T. Structure and Dynamics of Halogenoethanol−Water Mixtures Studied by Large-Angle X-ray Scattering, Small-Angle Neutron Scattering, and NMR Relaxation. *J. Phys. Chem. A* **2005**, *109*, 7667−7676.
(36) Chitra, R.; Smith, P. E. Properties of 2,2,2-trifluoroethanol and water mixtures. *J. Chem. Phys.* **2001**, *114*, 426.
(37) Singh, P. C.; Inoue, K.-i.; Nihonyanagi, S.; Yamaguchi, S.; Tahara, T. Femtosecond Hydrogen Bond Dynamics of Bulk-like and Bound Water at Positively and Negatively Charged Lipid Interfaces Revealed by 2D HD-VSFG Spectroscopy. *Angew. Chem., Int. Ed.* **2016**, *55*, 10621−10625.
(38) Singh, P. C.; Nihonyanagi, S.; Yamaguchi, S.; Tahara, T. Interfacial water in the vicinity of a positively charged interface studied by steady-state and time-resolved heterodyne-detected vibrational sum frequency generation. *J. Chem. Phys.* **2014**, *141*, 18C527.
(39) Singh, P. C.; Nihonyanagi, S.; Yamaguchi, S.; Tahara, T. Communication: Ultrafast vibrational dynamics of hydrogen bond network terminated at the air/water interface: A two-dimensional heterodyne-detected vibrational sum frequency generation study. *J. Chem. Phys.* **2013**, *139*, 161101.
(40) Singh, P. C.; Nihonyanagi, S.; Yamaguchi, S.; Tahara, T. Ultrafast vibrational dynamics of water at a charged interface revealed by two-dimensional heterodyne-detected vibrational sum frequency generation. *J. Chem. Phys.* **2012**, *137*, 094706.
(41) Abraham, M. J.; van der Spoel, D.; Lindahl, E.; Hess, B.; The GROMACS Development Team. Gromacs User Manual 5.1.4. www.gromacs.org, 2016.
(42) Duffy, E. M. *PhD. thesis*, Yale University, 1994.
(43) Gerig, J. T. Toward a Molecular Dynamics Force Field for Simulations of 40% Trifluoroethanol−Water. *J. Phys. Chem. B* **2014**, *118*, 1471−1480.
(44) Berendsen, H. J. C.; Postma, J. P. M.; van Gunsteren, W. F.; DiNola, A.; Haak, J. R. Molecular dynamics with coupling to an external bath. *J. Chem. Phys.* **1984**, *81*, 3684−3690.
(45) Parrinello, M.; Rahman, A. Polymorphic transitions in single crystals: A new molecular dynamics method. *J. Appl. Phys.* **1981**, *52*, 7182−7190.
(46) Frenkel, D.; Smit, B. *Understanding Molecular Simulation: From Algorithms to Applications*, 2nd ed.; Academic: San Diego, CA, 2002.
(47) Bader, R. F. W. *Atoms in Molecules - A Quantum Theory*, Oxford University Press: USA, 1990.
(48) Frisch, M. J.; Trucks, G. W.; Schlegel, H. B.; Scuseria, G. E.; Robb, M. A.; Cheeseman, J. R.; Scalmani, G.; Barone, V.; Mennucci, B.; Petersson, G. A.; et al. *Gaussian 09*, Revision B.01; Gaussian, Inc.: Wallingford, CT, 2010.
(49) Mondal, S.; Biswas, B.; Sarkar, S.; Singh, P. C. A combined molecular dynamics simulation, atoms in molecule analysis and IR study on the biologically important bulk fluorinated ethanols to understand the role of weak interactions in their cluster formation and hydrogen bond network. *J. Mol. Liq.* **2017**, *240*, 708−716.
(50) Ratajska-Gadomska, B.; Gadomski, W. Influence of confinement on solvation of ethanol in water studied by Raman spectroscopy. *J. Chem. Phys.* **2010**, *133*, 234505.
(51) Scharge, T.; Wassermann, T. N.; Suhm, M. A. Weak Hydrogen Bonds Make a Difference: Dimers of Jet-Cooled Halogenated Ethanols. *Z. Phys. Chem.* **2008**, *222*, 1407.
(52) Scharge, T.; Cézard, C.; Zielke, P.; Schütz, A.; Emmeluth, C.; Suhm, M. A. A peptide co-solvent under scrutiny: self-aggregation of 2,2,2-trifluoroethanol. *Phys. Chem. Chem. Phys.* **2007**, *9*, 4472−4490.

DOI: 10.1021/acs.jpcb.8b04365
J. Phys. Chem. B 2018, 122, 6616−6626